Optimal sensor placement for high pressure and low pressure EGR estimation

Author, co-author (Do NOT enter this information. It will be pulled from participant tab in MyTechZone)

Affiliation (Do NOT enter this information. It will be pulled from participant tab in MyTechZone)

Abstract

Low pressure exhaust gases recirculation (LP-EGR) is becoming a state-of-the-art technique for Nitrogen oxides (NOx) reduction in compression ignited (CI) engines. However, despite the pollutant reduction benefits, LP-EGR suffers from strong non-linearities and delays which are difficult to handle, resulting in reduced engine performance under certain conditions. Measurement and observation of oxygen concentration at the intake have been a research topic over the past few years, and it may be critical for transition phases (from low pressure to high pressure EGR). Here, an adequate selection of models and sensors is essential to obtain a precise and fast measurement for control purposes. The present paper analyses different sensor configurations, with oxygen concentration measurements at the intake and exhaust manifold and combines observation techniques with sensor models to determine the potential of each configuration. Experimental results from a 2.2 l. diesel engine are used to validate the presented techniques.

Introduction

During recent years, different technologies have been developed to reduce emissions on CI engines. NOx emissions are particularly detrimental to human health so there is continued research on how to improve the design of diesel engines as current emission legislation becomes stricter. To this matter, EGR systems have proven to be a particularly effective strategy to reduce NOx emissions through the reduction in oxygen concentration and combustion temperature [1][2][3]. There are two main EGR configurations, high pressure EGR and low pressure EGR. HP-EGR is the most widely used system due to its simpler layout and because it can provide high EGR rates with faster dynamics than other EGR systems, especially at lower speeds and loads [2][4][5]. On the other hand, LP-EGR ensures an adequate mixture of exhaust gases and air before entering the cylinders and it also manages lower temperatures and pressure than HP-EGR, which might improve the trade-off between NOx and efficiency. However, it has slower dynamics and it usually requires an additional valve to ensure positive differential pressure between the turbine outlet and the compressor inlet [2][5][6][7][8].

To have the benefits of both systems, current research efforts are focused on developing dual-loop EGR systems. Dual-loop EGR allows the engine to conduct multiple combustion modes and to reduce its emissions. Many authors are investigating the potential effects of implementing this system in a diesel engine. Experimental results showed that the addition of LP-EGR in a dual-mode system can lead to high efficiency and clean combustion under various operating conditions. In [8] a 6% CO_2 reduction was achieved with the addition of the LP-EGR loop, while in [9] a reduction between 51% and 64% for NOx emissions was obtained (referring to the standard engine behaviour in Euro 5 configuration). In [10], the authors showed an improvement in brake thermal efficiency when using dual-loop EGR in all the conditions tested.

EGR rate demand is an important factor when choosing the EGR system as the oxygen availability is critical for the in-cylinder combustion phasing. However other thermodynamic properties, such as the pressure or the temperature are also affected at the intake and exhaust manifold, which are also important for the complete cycle. In [11], the authors developed different control strategies and studied the interactions between systems. Research was also made through numerical simulations: in [12], the authors studied the wave motion in the intake and the exhaust systems, both with steady and transient conditions using a 1D thermo-fluid dynamic model, while in [13] the HP/LP split effects on the engine performance and emissions were simulated at steady state conditions using a 1D engine model based on experimental conditions.

The engine performance and emissions are affected by different parameters along the airpath. The models of the airpath increase in complexity as dual-mode EGR loops are considered. To have proper control of the combustion process, the in-cylinder oxygen availability must be correctly estimated. Concretely, transient conditions are critical, as the difference between the response time of the air path system and the combustion system becomes relevant. In this regard, [14] developed an algorithm to estimate the EGR mixing and transport delay of the LP- EGR system from a SI engine, where oxygen sensors were located along the airpath and were used to validate the results. In [15] the authors investigate Universal Exhaust Gas Oxygen (UEGO) sensors and their potential to be used for measuring the oxygen concentration in the intake manifold, particularly to estimate the EGR rate. Some works, such as [16][17], made use of the mass transport phenomena to estimate the burned gas ratio time delay, by relating the gas speed along the intake line with the mass flow rates and the thermodynamics conditions. While others developed a mean-value model using filling and emptying concepts for the manifolds, e.g. [18] with a variable-geometry turbocharger (VGT) and exhaust gas recirculation (EGR) in a diesel engine. They proposed a model with eight states, including the pressure and the oxygen mass fraction for each manifold. Their model was validated both with dynamic and stationary measurements. Observer-based estimations were also used in [19] for estimation of the intake air mass for a SI engine using an Extended Kalman Filter, or in [20] where the authors also used an EKF applied to a light-duty diesel engine, creating 8 sub-models to estimate the air system states.

Although the dual-loop system shows many advantages, it also brings some inconveniences that should be solved to continue improving this technology. On the one hand, it is difficult to directly measure the EGR mass flow rate since sensors are not available in production engines. On the other hand, there are the system dynamics, each line has different dynamics which leads to a highly coupled nonlinear airflow system when both configurations are used. Therefore, this study aims to assess how different sensor configurations may affect the estimation accuracy of some engine parameters, such as the EGR rate, by identifying the corresponding delays in each subsystem of the air path. Finally, an observer (Kalman filter) is designed based on the developed models and the results are compared to experimental data obtained from a 2.2l CI engine.

This paper is organized as follows: the first section presents the experimental setup as well as the experimental campaign. In the second section, the main theoretical models are presented, which will be used in the third section to feed an observer by taking several hypotheses and considering a few realistic sensor data sets. The results are then presented to validate the proposed methodology and, finally, in the last section, some conclusive remarks are given.

Tools

Experimental Setup

Experimental tests were carried out in a four-cylinder diesel engine with 2.2 l of total displacement, its main specifications are summarized in Table 1. The engine is equipped with a turbocharger and a HP-EGR line. Additionally, a LP-EGR line was incorporated into the engine on a test cell along with two actuators: the LP-EGR valve and the back-pressure valve (BP valve). The LP-EGR is located after the particulate filter and before the exhaust BP valve and is introduced at the compressor inlet location (Figure 1).

Table 1: Engine specifications

Description	Units	Value
Displaced volume	[cc]	2179
Stroke	[mm]	96
Bore	[mm]	85
Compression ratio	[-]	16:1
Cycle	[-]	4-stroke

Experimental pressure and temperature sensors were installed on the engine for air system modelling and validation. For temperature sensors, type 'K' thermocouples are being used, while the pressure sensors are piezoresistive sensors with different ranges according to their position on the engine. Two smart NOx sensors were also installed on the air path, one before the compressor inlet and the other just before the intake manifold to track NOx and O2 species along the intake line and provide insight on LP-EGR transport. A complete scheme of the experimental test bench is shown in Figure 1.

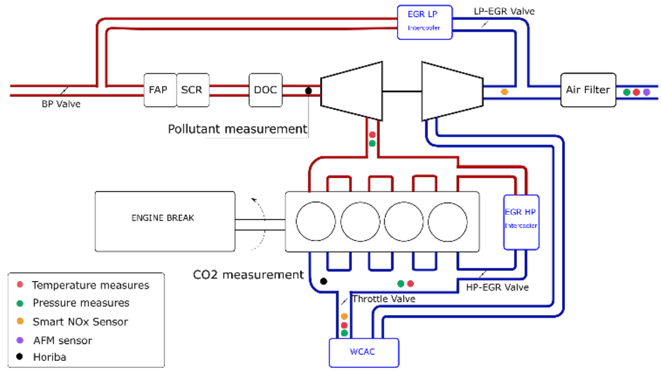

Figure 1: Engine Layout

As for the control architecture, measurements coming from the ECU, the test cell and the additional sensors employed were recorded by different acquisition systems. A STARS acquisition system was used to collect all test cell sensors with an acquisition rate of 10 Hz. An ETAS system was programmed to connect with the ECU and download a selected set of variables from the ECU at 100 Hz. A PXI-RT system was employed for acquiring and processing the data from the NOx sensors and the cylinder pressure signals, which require high acquisition rates. In-cylinder pressure was acquired at 0.5 CAD/sample. All systems were synchronized by a clock signal sent from PXI to STARS. The LP-EGR valve and the BP valve were controlled using a slave FPGA controlled by the PXI. The HP-EGR valve was controlled through ASAM3 protocol. This architecture is illustrated in Figure 2.

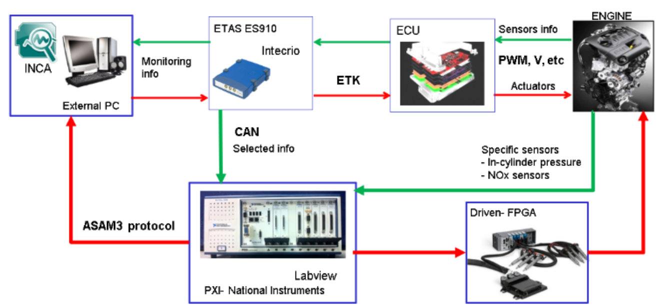

Figure 2: Control architecture

1D engine model

Despite the exhaustive instrumentation of the engine depicted in Figure 1, the limited number of sensors and their spatial and temporal resolution limitations makes the use of physical-based models, with a high degree of accuracy, essential to understanding and providing a physical interpretation to the complex and non-linear dynamic phenomena involved in the ICE, particularly in its gas exchange process. To this aim, an in-house high fidelity engine model (VEMOD) has been used. VEMOD is based on physical submodels of different engine systems (block and cylinders, turbocharger, coolers, pumps, exhaust line and ducts), it considers the interaction between the gas, coolant and oil circuit to evaluate the effect of different mechanical definitions on consumption, emissions and thermal behaviour. The air-path is modelled through the combination of a 1D gas dynamics model, which calculates the flow properties in the intake, exhaust, high and low pressure EGR ducts, and submodels of elements such as compressor, turbine, heat exchangers or valves, some of them, mainly based on experimental information, e.g., compressor or turbine maps. The gas dynamics model is coupled with a cylinder model that predicts the evolution of the in-cylinder gas properties using a physical combustion model based on the turbulent gas jet theory [21], and state of the art modelling of the heat transfer. The engine model has been calibrated with the geometrical characteristics of the engine described in Table 1 and with experimental data in steady and transient conditions. A detailed description of the model is available at [22].

Considering the dynamic limitations of the gas concentration sensors (lambda sensor, smart NOx sensor and gas analyser), VEMOD has been used to characterize the LPEGR and exhaust lines to assess the main dynamic characteristics of the process (delay and time response) and provide insight into real-time capable modelling options.

Test methodology

Two types of transient tests will be used in this work to calibrate and validate the models and the observer.

1. EGR steps: Steps with HP-EGR, LP-EGR, and VGT were performed separately at 2500 rpm and 110 Nm to analyse the dynamic response of the system. Figure 3 shows the EGR valves position during this test, as well as the VGT and BP valves position. It should be noted that the BP valve was only used after the LP-EGR valve reached its maximum value.

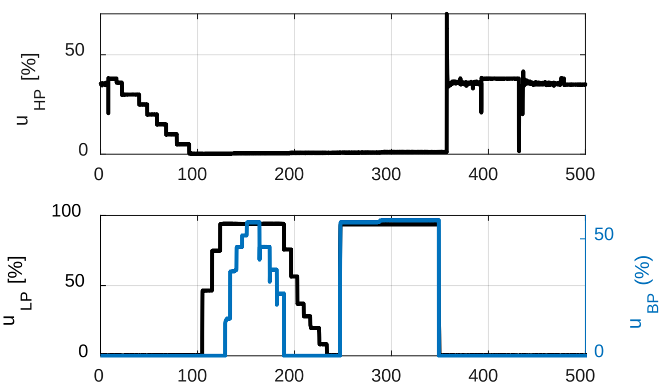

Figure 3: Calibration test

2. Tip-in: To evaluate the performance of the observer, four different tests were performed at 2500 rpm from 110Nm to 150Nm: the first test consists in a load step with HP-EGR, the second one a similar step with LP-EGR and the last two tests consisted in different strategies to control a transition between medium load with HP-EGR to high load with LP-EGR conditions. The strategies were automatized in the ECU while the LP-EGR valve was controlled by full-pass. In the first strategy, the LP-EGR valve opens just after the HP-EGR valve is closed. The second strategy was designed to optimize the overshoot of O2 and intake pressure by acting first on the LP-EGR valve, i.e., small phasing difference between the EGR valves of 400 ms and using the VGT to compensate the effects of the step. Figure 4 illustrates the tests performed.

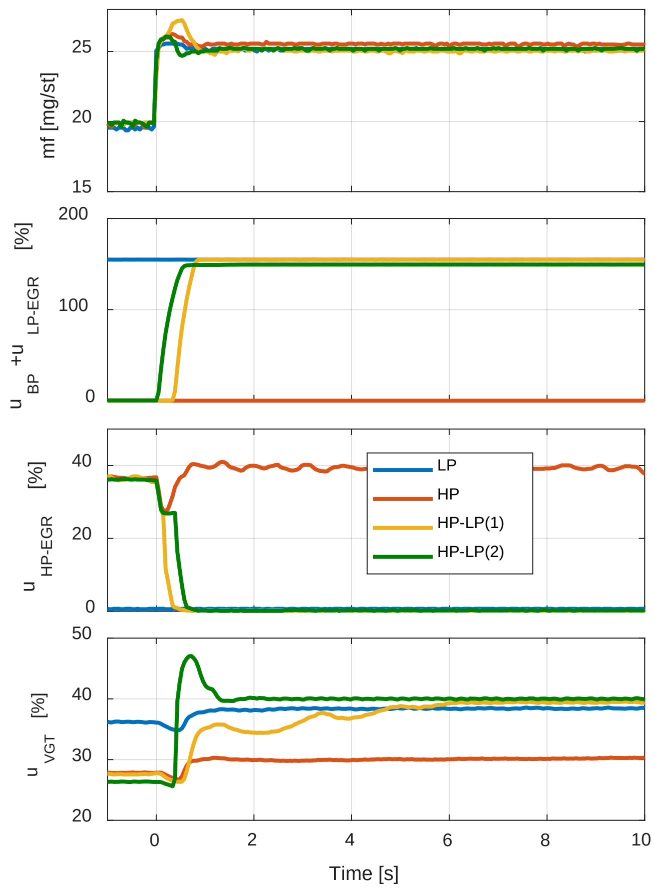

Figure 4: Tip in tests at 2500 rpm, from110 Nm to 150 Nm

Model description

To estimate the oxygen mass concentration, different sensors at the airpath are combined with dynamic and static models to have a robust and fast measurement at any conditions. In this section, a review of the models used is presented.

EGR valves

Both EGR valves (LP and HP) will be modelled as an isothermal orifice, considering the flow through the valves as compressible and neglecting the pressure recovery after the orifice. Then, the mass flow through the valves is estimated as in equation 1. The effective opening of the valve (A_{egr}) is obtained empirically as a function of the EGR valve position (u_{EGR}). The expansion factor (Ψ_{egr}) is a function of the pressure ratio $\Pi_{EGR} = p^{us}/p^{ds}$.

$$W_{egr} = A_{egr}\Psi_{egr}\frac{p^{us}}{\sqrt{RT^{us}}} \tag{1}$$

$$\psi_{EGR} = \begin{cases} \sqrt{\gamma\left(\frac{2}{\gamma+1}\right)^{\frac{\gamma+1}{\gamma-1}}} & if\ \pi_{EGR} \leq \pi_{cr} \\ \pi_{EGR}^{\left(-\frac{1}{\gamma}\right)}\sqrt{\frac{2\gamma}{\gamma+1}\left(1-\pi_{EGR}^{\frac{1-\gamma}{\gamma}}\right)} & if\ \pi_{EGR} \leq \pi_{cr} \end{cases} \tag{2}$$

Where the critical pressure ratio (π_{cr}) is a function of the adiabatic factor (γ) as in equation 3.

$$\pi_{cr} = [(0.5)(\gamma+1)]^{\frac{\gamma}{\gamma+1}} \tag{3}$$

The pressure and temperature upstream of the valve, p^{us} and T^{us}, and the pressure downstream of the valve, p^{ds}, are collected from sensors in the engine.

In both EGR valves, the temperature sensor can be substituted using the heat exchanger efficiency as a function of the EGR mass flow, and the measurement provided by a temperature sensor at the exhaust:

$$T_{EGR}^{ds} \cong T_{em} - \eta_{int}(W_{EGR})(T_{em} - T_w) \tag{4}$$

The pressure downstream of the LP-EGR valve is computed from the pressure sensor upstream of the compressor, considering that the pressure (p^{ds}) must be between the atmospheric pressure and that value. A correction factor is applied to consider the losses at the line as a function of the air mass flow.

$$p_{lp}^{ds} \cong k_C(W_{air})p_C^{us} + (1 - k_C(W_{air}))p_{atm} \tag{5}$$

The pressure upstream of the LP EGR valve can be estimated from a sensor located at the valve, that can be also used to estimate the pressure at the upstream of the back-pressure valve, while the pressure near the HP valve can be directly obtained from the intake and exhaust manifold, by neglecting any pressure losses at the HP-EGR line.

$$p_{hp}^{us} \cong p_{em} \tag{6}$$

$$p_{hp}^{ds} \cong p_{im} \tag{7}$$

Intake Manifold dynamics

The dynamics at the intake process can be represented by an emptying and filling model. The models are then derived from the mass and energy equation applied to a control volume. Assuming an adiabatic process and a perfect gas mixture composition. Equations 8-9 represent the pressure and oxygen concentration variations at the intake manifold

$$\dot{p}_{im} = \frac{\gamma R}{V_{im}}\left(W_c T_c + W_{hp} T_{hp} - W_{im} T_{im}\right) \tag{8}$$

$$\dot{F}_{im} = \frac{T_{im} R}{p_{im} V_{im}}(F_C W_C + F_{HP} W_{HP} - F_{im} W_{im}) \tag{9}$$

where F_{im} is the relative oxygen concentration (F=X_{O2}/X_{O2}^{atm}) at the intake, V_{im} is the intake manifold volume, η_v is the volumetric efficiency which is usually in a range between 0.8 to 0.95, V_{dis} is the engine displacement, and W_{hp} is the HP-EGR mass flow at the intake manifold. The speed-density method (Eq.10) was used to calculate the intake mass flow, and the temperature at the intake manifold was estimated from the temperature at the water charge cooler (Eq. 13).

$$W_{im} = \frac{\eta_v T_{im} R}{p_{im} V_{dis}} \frac{N}{120} \tag{10}$$

$$T_{im} = \frac{(T_{WCAC} W_c + T_{hp} W_{hp})}{W_c + W_{hp}} \tag{11}$$

where N is the engine speed in rpm.

The oxygen availability at the exhaust manifold can be obtained from the oxygen at the intake by removing the oxygen consumed at combustion,

$$F_{em} = \frac{F_{im} W_{im} - AFR_{st} W_f}{W_{im} + W_f} \tag{12}$$

LP-EGR line dynamics

While the EGR valve model represented by equations 1 and 2 is the standard approach to model the HP-EGR flow, the time needed for exhaust gas species to cover the distance between the exhaust and intake manifold with LP-EGR can lead to substantial errors if it is assumed that the flow calculated in the LP-EGR instantaneously reaches the intake manifold. Complex phenomena involved in the gas transport between the exhaust and intake manifolds via the LP-EGR system require detailed models such as the 1D approach, which are outside of the computation capabilities of on-board control systems. To handle the complex transport phenomena, a black box dynamic model was proposed to estimate the transport and diffusion of species at the intake, LP-EGR and exhaust lines. In this section, the LP-EGR path dynamics will be characterized by the transient analysis of O2 concentrations at different points in the air path due to the availability of lambda/smart NOx sensors. On the one hand, gas transport from the turbine outlet, where the exhaust O2 sensor is placed, to the LP-EGR outlet should be considered. It will be assumed that along this path the gas does not suffer any substantial modification in its composition, which at least from the O2 point of view seems reasonable. On the other hand, the gas is also transported from the LP-EGR outlet to the intake manifold, of course, in this case in addition to the transport, there would be changes in the measured composition due to the mixing with fresh air along the intake line. In this sense, two different gas transport will be considered: from the turbine outlet to the LP-EGR outlet and from the LP-EGR outlet to the intake manifold.

Transient data from the 1D model previously presented (VEMOD) has been used to identify different black-box models and evaluate their trade-off between accuracy and complexity. The following three approaches have been evaluated:

a) Variable transport delay: The simplest case of fluid transport would consist of a flow with constant density and no diffusion. If additionally, constant mass flow is considered, an eventual signal measuring the concentration of a given specie at the inlet will be transported to the outlet without distortion. Let u be the O2 concentration signal at the start of the line (e.g., VGT outlet where the exhaust lambda sensor is placed), and y the O2 concentration at the end of the considered line (e.g., at the LP-EGR valve), then, considering the previous assumptions:

$$y_t = u_{t-\delta_t} \tag{13}$$

where subindex t represents the current time and δ is the lag representing the time needed to cover the path distance. In general, δ will vary over time, since it depends on the mass flow that, in the considered application, would vary with time and can be assumed proportional to the engine speed since the engine is a volumetric machine. Note that the variations in δ will lead to some distortion in the signal. The following expression for δ is proposed:

$$\delta_t = \frac{k}{n} \tag{14}$$

where k represents a non-dimensional constant to be identified, related to the ratio between the pipe volume and the engine displacement.

The O2 concentration at VGT outlet, LP-EGR outlet, compressor inlet and intake manifold obtained from VEMOD simulations of transient cycles have been used to identify the model. Signals at the VGT and LP-EGR outlet are used to estimate the delay of the exhaust line, while compressor inlet and intake manifold signals are used to estimate the lag of the intake line. Note that compressor inlet signal is used instead of LP-EGR outlet signal to assure high correlation between signals. The method used to find the delay consists of searching the shift in the input signal (u) that maximizes the cross-correlation between signals. To obtain a variable delay, a moving window of 10s is used to estimate the correlation between signals. Figure 5 shows the delay obtained in the intake line during the considered cycle by applying the previous method, according to the engine speed. One can observe that results follow a clear trend, that allows identifying k in equation 14. In addition, results show that the lag in the intake line is in the range of 0,2 to 0,6 seconds for this engine, pointing out that LP-EGR transients will be especially critical at low engine speeds.

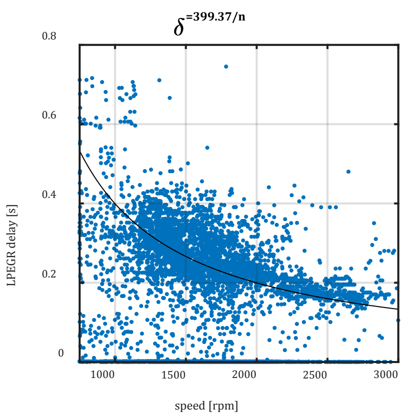

Figure 5. LP-EGR delay at the intake line.

b) Variable transport delay plus first-order dynamics: The strong simplification hypothesis of the previous approach suggests that some dynamic correction is needed to handle the distortion due to complex fluid dynamics. In this sense, one may think of adding a first-order system that represents the accumulations that can appear in the line volumes. According to this idea, the model proposed would be:

$$\frac{dy_t}{dt} = \frac{1}{\tau}\left(u_{t-\delta_t} - y_t\right) \tag{15}$$

Where τ is the time constant to calibrate, which is related to the volume of elements with accumulation capabilities in the line. The VEMOD data during transients has been used to identify the value of τ that minimizes the quadratic error of the model.

c) First-order dynamics: the second model (b) will improve the first model (a) for obvious reasons (equation 15 contains equation 13). However, both models share the transport delay or deadtime, which leads to control and observation issues as the deadtime should pass before getting any feedback. For this reason, in this approach a simple first-order dynamic system is proposed:

$$\frac{dy_t}{dt} = \frac{1}{\tau}(u_t - y_t) \tag{16}$$

Figure 6 shows the O2 evolution in the intake manifold during a segment of the modelled cycle for the three models previously presented. The signals in the compressor inlet and intake manifold are also included to allow a fair comparison. One can observe that the application of model (a) substantially improves the estimation of the O2 in the intake manifold compared to the one that can be obtained with the concentration at compressor inlet (this could be representative of what should be obtained with equations 1 and 2 applied to the LPEGR valve). Adding first-order dynamics slightly improves the accuracy as shown by the model (b) results. Finally, using a simple first-order system provides notable improvements in comparison to using the compressor inlet estimation but does not reach the level of representativity of models (a) and (b).

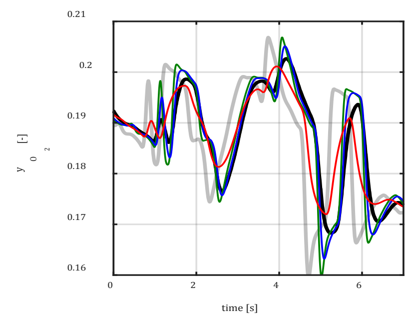

Figure 6. Comparison between O2 mass concentration in the compressor inlet (grey), intake manifold (black), intake manifold estimated with model (a) in green, model (b) in blue and model (c) in red.

Finally, Figure 7 shows the cumulative probability distribution of the absolute value error in the O2 concentration at the intake manifold estimated by the models previously presented. A similar analysis can be obtained for the exhaust line lag (between VGT outlet and LPEGR outlet). Model (c) represented by equation 16, has been chosen for this work due to the important improvement regards the option without considering dynamics (compressor inlet) and simplicity in the observer development, despite leading to higher errors than the first model.

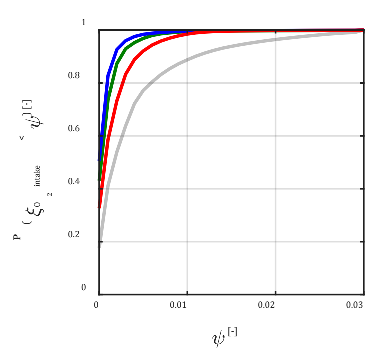

Figure 7: Cumulative probability distribution of the error in the O2 concentration at the intake manifold estimated by O2 mass concentration in the compressor inlet (grey), model (a) in green, model (b) in blue and model (c) in red.

Sensor dynamics

Most of the sensors, such as in-cylinder pressure sensors, can be considered instantaneous, as the measurement given by the sensor represents the thermodynamic property observed. However, because of the working principle, sensors use to exhibit a characteristic time response, which can range from few ms, such as in air mass flow meters, to few seconds, such as some temperature sensors.

The response of the sensor in the time domain can be described as a first order system:

$$\frac{dx_t}{dt} = \frac{1}{\tau}(u_t - x_t) \tag{17}$$

where x is the sensor signal and u its excitation. The thermocouples at the exhaust line are Type K with a diameter of 3mm, while other thermocouples at the intake have a diameter of 1,5 mm. The expected time response from the manufacturer information is 15 and 5 seconds, respectively. Which agrees with the expected time response observed. The smart NOx sensors are expected to have a characteristic time response of 900 ms, while the gas analyser that measures the oxygen concentration at the intake and exhaust has a characteristic time of a few seconds. The rest of the sensors used, namely pressure sensors and hot film anemometer, are considered instantaneous, as its time response is below the discretization time (1 cycle).

Sensor set and model calibration

The selection of the sensors and models represents a trade-off between the precision and time response of the final measurement and the cost of the complete control system. In the present work the minimum set of sensors selected are:

- Three pressure sensors: at the inlet of the compressor, at the intake manifold, and near the inlet of the LP-EGR valve (a differential pressure can be also used).
- A Temperature sensor at the exhaust line
- A hot-film anemometer at the intake

This set of sensors can be commonly found in CI commercial engines.

The volumetric efficiency has been characterized with the air mass flow meter with no EGR conditions, while the calibration of the EGR valves was obtained by assuming constant volumetric efficiency at EGR steps by maintaining the rest of the operating conditions steady. Figure 8 shows the result of the speed density method and the result of both EGR valves and the air mass flow sensor.

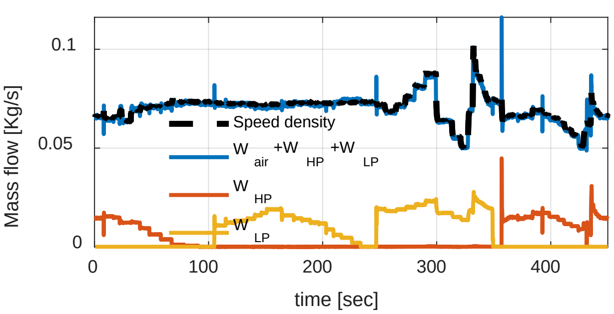

Figure 8: Speed density and EGR valve models under steps of EGR and VGT at 2500 rpm and 110 Nm (steps shown in Figure 3)

The temperature at both EGR valves has been obtained from the exhaust manifold temperature by using a variable efficiency as a function of the EGR flow, such as (Eq. 4). If a temperature sensor is available near the valve, an independent observer can be also used to consider the temperature sensor dynamics and update the model. The pressure at the outlet of the LP-EGR valve was obtained from the pressure sensor at the inlet of the compressor following Eq. 5. Figure 9 shows the result of the models, together with sensors located near the valve when performing HP and LP steps at 2500 rpm.

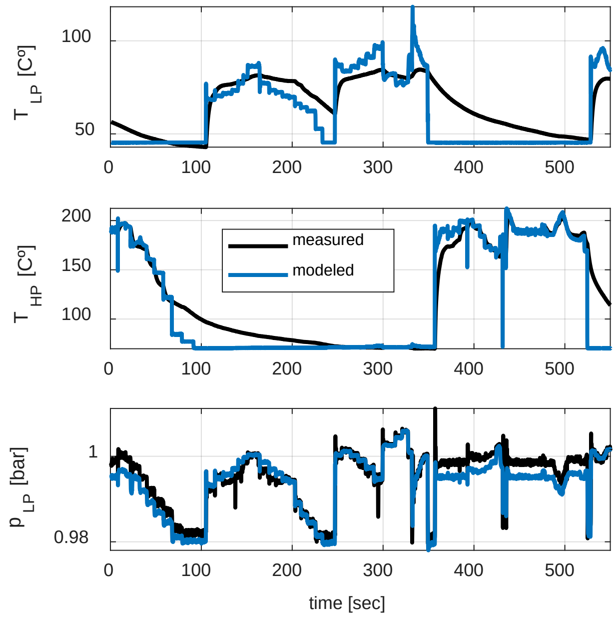

Figure 9: Measured versus model results for the LPEGR outlet temperature (top), HPEGR outlet temperature (centre) and LPEGR outlet temperature (bottom).

In the present study the use of the intake manifold temperature sensor, as well as the use of oxygen concentration sensors (smart NOx sensors) were studied. The possible locations for the oxygen concentration are:

- **Before the compressor inlet**: to avoid pressure corrections at the lambda signal and to provide measurements of the LP-EGR
- **After the HP-EGR valve**: to measure both, LP and HP-EGR mass flows.
- **At the intake manifold**: just before the HP valve, to ensure an adequate measurement of the LP and avoid inhomogeneities coming from HP-EGR flow.
- **At the exhaust**: to improve the estimation of oxygen concentration at the exhaust.

Because of incomplete mixing the two first locations were discarded as they did not provide satisfactory results in steady conditions due to the lack of composition homogeneity, i.e., the first one only detected a 30% of the expected LP-EGR flow, while the second one overestimated the EGR at some conditions in a 28 % of the total EGR.

Observer Design

The observer was designed by applying finite differences with a discretization time of one cycle. The objective of the observer is to combine all the sensor and model information and update the speed density and the EGR valve models when they bias from the expected response. Henceforth, three states correspond to the volumetric efficiency (η_v), a correction over the HP-EGR valve (K_{HP}), and a correction over the LP-EGR valve (K_{LP}), which should be constant if no model deviation is observed.

$$\eta_v^{k+1} = \eta_v^k \quad (18)$$

$$K_{LP}^{k+1} = K_{LP}^k \quad (19)$$

$$K_{HP}^{k+1} = K_{HP}^k \quad (20)$$

Following the results obtained from VEMOD, a first order system was used to represent the dynamics between the flow at the LP-EGR valve, and the flow at the intake manifold:

$$W_C^{k+1} = W_C^k k_{fC} + (1 - k_{fC})(W_{air}^k + W_{LP}^k K_{LP}^k) \quad (21)$$

Where W_{air}^k and W_{LP}^k are inputs obtained from the air mass flow sensor and the LP-EGR valve model, respectively.

The temperature at the intake manifold is obtained from the temperature at the water charge cooler and the temperature of the HP-EGR flow by thermodynamic equilibrium.

$$T_{im}^{k+1} = \frac{T_{WC}^k W_C^k + T_{HP}^k W_{HP}^k K_{HP}^k}{W_C^k + W_{HP}^k K_{HP}^k} \quad (22)$$

Where the temperature of the water charge cooler can be considered constant and W_{HP}^k is derived from the HP-EGR valve model.

The mass flow dynamics are modelled with the adiabatic intake manifold:

$$p_{im}^{k+1} = p_{im}^k + \Delta t^k \frac{\gamma R}{V_{im}} (W_C^k T_{WC}^k + K_{HP}^k W_{HP}^k T_{HP}^k - W_{im}^k T_{im}^k) \quad (23)$$

Where N is the engine speed in *rpm* and W_{im}^k is a function of the volumetric efficiency and the conditions at the intake manifold:

$$W_{im}^k = \frac{\eta_v^k V_{dis} p_{im}^k}{R T_{im}^k} \frac{N^k}{120} \quad (24)$$

The oxygen concentration at the intake manifold is considered by:

$$F_{im}^{k+1} = F_{im}^k + \Delta t^k \frac{R T_{im}^k}{p_{im}^k V_{im}} (W_C^k F_C^k + K_{HP}^k W_{HP}^k F_{HP}^k + F_{im}^k W_{im}^k) \quad (25)$$

The exhaust manifold oxygen concentration is updated from the intake manifold estimation:

$$F_{em}^{k+1} = \frac{F_{im}^k W_{im}^k - AFR_{st} W_f^k}{W_{im}^k + W_f^k} \quad (26)$$

Where AFR_{st} is the stoichiometric air to fuel ratio, i.e., 14.6 in the present work, and W_f^k the fuel mass flow.

The oxygen concentration at the LP-EGR valve is assumed to be represented by a first order system, characterized by k_{fE} following the hypothesis of first order transport used for the intake line, such as:

$$F_{LP}^{k+1} = k_{fE} F_{LP}^k + (1 - k_{fE}) F_{em}^k \quad (27)$$

And the mixture of the air with the LP-EGR flow is represented by:

$$F_C^{k+1} = k_{fC} F_C^k + (1 - k_{fC}) \frac{F_{em}^k W_{LP}^k K_{LP}^k + W_{air}^k}{W_{LP}^k K_{LP}^k + W_{air}^k} \quad (28)$$

Finally, the sensors time response has been modelled with their characteristic constants (k_{fS1}, k_{fS2}, and k_{fS3})

$$T_{S,im}^{k+1} = k_{fS1} T_{S,im}^k + (1 - k_{fS1}) T_{im}^k \quad (29)$$

$$F_{S,C}^{k+1} = k_{fS2} F_{S,EM}^k + (1 - k_{fS2}) F_C^k \quad (30)$$

$$F_{S,EM}^{k+1} = k_{fS3} F_{S,EM}^k + (1 - k_{fS3}) F_{em}^k \quad (31)$$

The resulting state space model is composed of 13 states, 4 outputs, and 7 inputs:

$$x_k = \begin{pmatrix} \eta_v^k \\ K_{LP}^k \\ K_{HP}^k \\ W_C^k \\ T_{im}^k \\ p_{im}^k \\ F_{im}^k \\ F_{em}^k \\ F_{LP}^k \\ F_C^k \\ T_{S,im}^k \\ F_{S,C}^k \\ F_{S,EM}^k \end{pmatrix}, y_k = \begin{pmatrix} p_{im}^k \\ T_{S,im}^k \\ F_{S,C}^k \\ F_{S,EM}^k \end{pmatrix}, u_k = \begin{pmatrix} W_{air}^k \\ W_{LP}^k \\ W_{HP}^k \\ T_{WC}^k \\ T_{HP}^k \\ W_f^k \\ N^k \end{pmatrix}$$

An extended Kalman filter (EKF) is proposed by linearizing the equations and using the conventional KF optimization procedure:

$$x_{k,k-1} = f(x_{k-1}, u_k) \quad (32)$$

$$e_k = y_k - g(x_{k,k-1}, u_k) \quad (33)$$

$$x_{k,k} = x_{k,k-1} + K_k e_k \quad (34)$$

Where $f(x_{k-1}, u_k)$ and $g(x_{k,k-1}, u_k)$ are the models previously described, and K_k is the Kalman gain, which is updated as follows:

$$P_{k,k-1} = F_k P_{k-1} F_k^T + Q_k \quad (35)$$

$$K_k = P_{k,k-1} H_k^T (H_k P_{k,k-1} H_k^T + R_k)^{-1} \quad (36)$$

$$P_k = (I - K_k H_k) P_{k,k-1} \quad (37)$$

Where F_k and H_k are the state transition and the observation matrices, which are obtained after linearizing f and g. Q_k and R_k are the covariance matrices of the process and the observation noise, which represent the reliability of each equation. P_k is the estimate covariance matrix which deals with the current estimation of the Kalman filter.

Results and Discussion

The process covariance was chosen to provide the EKF with sufficient robustness even when it is highly perturbed. The values chosen are collected in Table 2

Table 2: Values used for the process covariance matrix

Variable	Unit	Value
$Q_{1,1}$	-	0.005
$Q_{2,2}$	%	2
$Q_{3,3}$	%	2
$Q_{4,4}$	kg/s	0.01
$Q_{5,5}$	K	5
$Q_{6,6}$	mbar	10
$Q_{7,7}$	%	5
$Q_{8,8}$	%	5
$Q_{9,9}$	%	5
$Q_{10,10}$	%	1
$Q_{11,11}$	K	5
$Q_{12,12}$	%	1
$Q_{13,13}$	%	1

The observer was first used with all sensors, i.e., intake pressure, intake temperature, oxygen concentration at intake, and oxygen concentration at the exhaust, with a covariance observation matrix derived from an expected noise value of 1 mbar, 5 K, 1%, and 1%, respectively.

Figure 10 shows the results of the Kalman filter in the four tests presented. The top plot shows the indicated mean effective pressure IMEP, computed as:

$$IMEP = \frac{\int pdV}{V_{dis}} \tag{38}$$

The second plot shows the output of the Kalman filter for the relative intake oxygen concentration. The third plot shows the CA90, which was estimated from the apparent heat release. The apparent heat release rate (AHRR) was computed from the in-cylinder pressure sensor and the volume estimation, such as:

$$AHRR = \frac{\kappa}{\kappa - 1} pdV + \frac{1}{\kappa - 1} Vdp \tag{39}$$

where κ can be considered constant. In this work, a value of 1.3 was used. Finally, the bottom plot shows the output of the NOx measurement located at the exhaust manifold.

In the first strategy tested to switch from HP to LP (open LPEGR at the same time that HPEGR is closed) the output of the EKF shows that the engine has several cycles (around 250 ms) without burnt gases in the cylinder, which agrees with the high peak of NOx measured and the overshoot measured at the IMEP and the CA90. In the second test switching from HP to LPEGR, the LPEGR valve is open and then the HPEGR valve closes to reduce such overshoot. Note also, that in the second strategy, as well as in the LP and HP tip-ins, the observer also detects a peak of the oxygen concentration when the tip-in is performed. This peak is caused by the intake manifold dynamics and the evolution of the concentration at the EGR and this result also agrees with a peak of NOx measured at the exhaust.

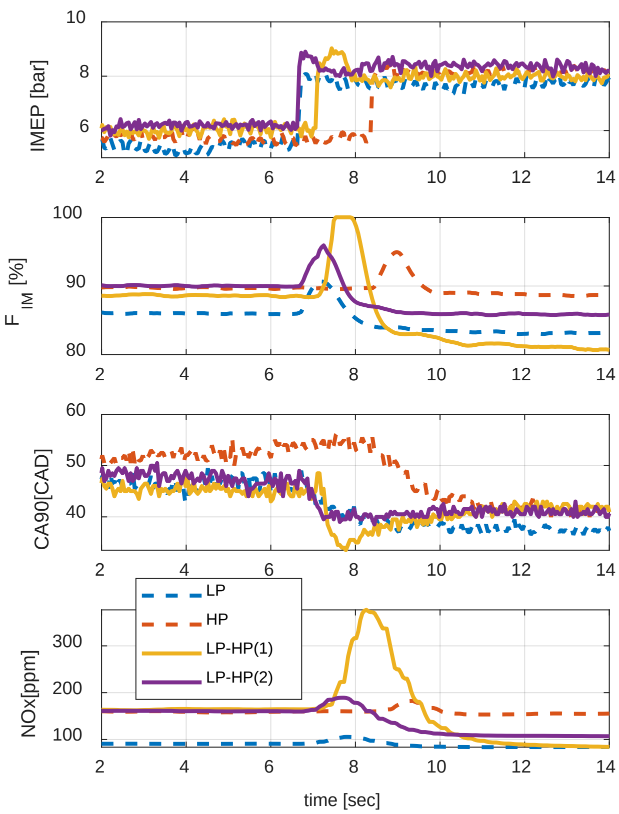

Figure 10: Results of Kalman filter on the four tip in tests

When the method capability to estimate the intake O2 concentration has been shown, different bias is introduced in the model parameters to assess the method robustness and its ability to use sensor information to compensate for those bias.

Three biases were simulated: at the volumetric efficiency, at the LP-EGR flow estimation, and at the HP-EGR flow estimation. The biases were introduced in the Kalman filter by multiplying the calibrated value of η_v^k, K_{LP}^k, and K_{HP}^kper 0.9.

The test selected for the analysis was the optimized strategy for the tip in transition between HP to LP. The EKF was first executed with no bias and by using all the sensor information. The result of such simulation was used as reference to estimate the error when bias is included, or some sensors are removed.

Figure 11 shows the response of the Kalman filter when the LP-EGR flow estimation was biased. In the top plot the evolution of the correction factor at the LP-EGR flow is shown, while in the bottom plot, the relative oxygen concentration at the intake is plotted in a continuous line with the reference value previously obtained when no bias was introduced.

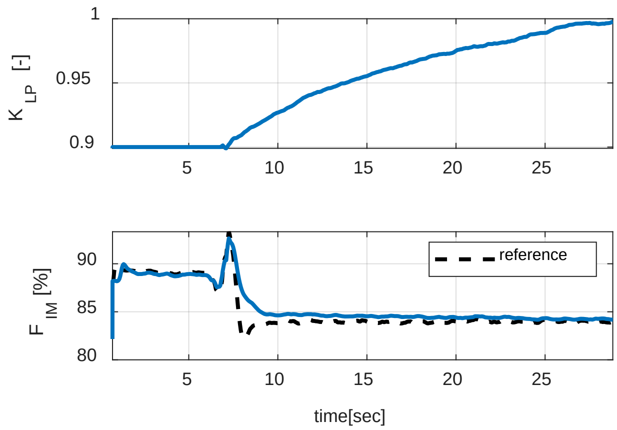

Figure 11: Example of EKF response with a bias at the LP-EGR flow estimation at HP-LP step

As it should be expected, the EKF does not correct the model till the LP-EGR starts. After the EGR switches, sensor information disagrees with the state space model. As a consequence, the objective of the observer is both, correct the bias and provide an estimation between the model prediction and the sensor value.

The Kalman filter was executed four times by introducing different noises associated at each measurement to neglect sensor information. The values used for the covariance observation matrix are tabbed in Table 3.

Table 3: Values used for EKF at various sensor configurations

Variable	Unit	All	F_{CO}	F_{em}	T_{im}
$R_{1,1}$	mbar	1	1	1	1
$R_{2,2}$	%	1	1	100	100
$R_{3,3}$	%	1	100	1	100
$R_{4,4}$	ºC	5	5000	5000	5

The differences found between the optimal estimation, i.e., no bias and all sensors used, and the rest of the combinations, are shown in Table 4. The positions marked in red indicate that the observer did not show a satisfactory trend to correct the bias.

Table 4: Errors found when biasing the calibrations used

Error (%)	All	F_{CO}	F_{em}	T_{im}
No bias	0	0.07	0.31	0.35
$\eta_v^0 = 0.9\eta_v^c$	1.81	1.85	2.88	2.88
$K_{LP}^0 = 0.9$	0.21	0.26	0.65	0.53
$K_{HP}^0 = 0.9$	0.25	0.78	0.53	0.5

An oxygen sensor located at the intake manifold would significantly reduce the error of the observation, especially when the LP-EGR is not accurately known, and it would be also beneficial to observe the volumetric efficiency. However, such a sensor cannot compensate for possible errors at the HP-EGR loop. These errors can be detected either by measuring the exhaust gases in transient conditions or by energy equilibrium at the intake with a temperature sensor.

Conclusions

An analysis of a dual EGR system was performed during the article. The research was focused on the determination of the oxygen concentration at the intake to provide the control system with a suitable measurement for optimizing the combustion. The experimental campaign was focused on transient tip-ins where HP-EGR at medium and low loads should be replaced by LP-EGR at high loads.

An observer was designed to offer an adequate transient estimation: the intake manifold dynamics were modelled by emptying and filling models, while the dynamics at the LP-EGR line were modelled by using a 1D simulation environment.

Experimental tests showed that the observer output for the oxygen concentration evolution explains the CA90 evolution and the exhaust NOx measured.

Regarding the required sensors for avoiding possible bias, different locations for lambda (or smart NOx sensors) were tested. Sensors located near the EGR valves did not offer satisfactory results, i.e. near the LP valve, only a 30% of the EGR was measured, which can be explained by incomplete mixing, while near the HP-EGR valve measurements differ from the expected value (around 28% in some conditions).

Finally, the optimal measurement with an adequate calibration and all sensors used was compared with the EKF output when biases are included. The EKF exhibits a positive trend to correct such bias when an oxygen concentration sensor at the intake, a lambda sensor at the exhaust and an intake temperature sensor are available. However, if some of the sensors are missing the EKF will not be able to compensate such errors.

References

[1] M. A. D. Gonzalez and D. Di Nunno, "Internal Exhaust Gas Recirculation for Efficiency and Emissions in a 4-Cylinder Diesel Engine," *SAE Tech. Pap.*, vol. 2016-Octob, 2016.

[2] M. S. Khalef, A. Soba, and J. Korsgren, "Study of EGR and Turbocharger Combinations and Their Influence on Diesel Engine's Efficiency and Emissions," *SAE Tech. Pap.*, vol. 2016-April, no. April, 2016.

[3] E. Schalk *et al.*, "Limits for NOX reduction by EGR in a heavy duty diesel engine at stationary and transient conditions," *ASME 2012 Intern. Combust. Engine Div. Fall Tech. Conf. ICEF 2012*, pp. 601–607, 2012.

[4] U. Asad and M. Zheng, "Exhaust gas recirculation for advanced diesel combustion cycles," *Appl. Energy*, vol. 123, pp. 242–252, 2014.

[5] O. Vítek, J. MacEk, M. Polášek, S. Schmerbeck, and T. Kammerdiener, "Comparison of different EGR solutions," *SAE Tech. Pap.*, vol. 2008, no. 724, pp. 776–790, 2008.

[6] G. F. Scocozza, N. Cavina, M. De Cesare, M. Panciroli, and C. Benedetti, "Experimental Investigation on the Effects of Cooled Low Pressure EGR and Water Injection on Combustion of a Turbocharged GDI Engine," in *SAE Technical Paper Series*, 2020, vol. 1.

[7] J. M. Luján, H. Climent, R. Novella, and M. E. Rivas-Perea, "Influence of a low pressure EGR loop on a gasoline turbocharged direct injection engine," *Appl. Therm. Eng.*, vol. 89, pp. 432–443, 2015.

[8] H. Lee, C. Jo, S. Yoon, S. Yi, Y. Kim, and J. Jeon, "Optimization of dual loop EGR of a V6 3.0 liter diesel engine for CO2 reduction," *SAE Tech. Pap.*, vol. 2, 2013.

[9] G. Zamboni, S. Moggia, and M. Capobianco, "Effects of a dual-loop exhaust gas recirculation system and variable nozzle turbine control on the operating parameters of an automotive diesel engine," *Energies*, vol. 10, no. 1, 2017.

[10] B. Mao, M. Yao, Z. Zheng, and H. Liu, "Effects of Dual Loop EGR and Variable Geometry Turbocharger on Performance and Emissions of a Diesel Engine," *SAE Tech. Pap.*, vol. 2016-Octob, 2016.

[11] F. Yan and J. Wang, "Design and robustness analysis of discrete observers for diesel engine in-cylinder oxygen mass fraction cycle-by-cycle estimation," *IEEE Trans. Control Syst. Technol.*, vol. 20, no. 1, pp. 72–83, 2012.

[12] L. Cornolti, A. Onorati, T. Cerri, G. Montenegro, and F. Piscaglia, "1D simulation of a turbocharged Diesel engine with comparison of short and long EGR route solutions," *Appl. Energy*, vol. 111, pp. 1–15, 2013.

[13] J. Park, S. Song, and K. S. Lee, "Numerical investigation of a dual-loop EGR split strategy using a split index and multi-objective Pareto optimization," *Appl. Energy*, vol. 142, pp. 21–32, 2015.

[14] F. Liu, J. M. Pfeiffer, R. Caudle, P. Marshall, and P. Olin, "Low Pressure Cooled EGR Transient Estimation and Measurement for an Turbocharged SI Engine," *SAE Tech. Pap.*, no. x, 2016.

[15] K. Hegarty, P. Dickinson, D. Cieslar, and N. Collings, "Fast O2 measurement using modified UEGO sensors in the intake and exhaust of a diesel engine," *SAE Tech. Pap.*, vol. 2, no. X, pp. 3–8, 2013.

[16] S. M. Hamze, D. Georges, E. Witrant, and D. Bresch-Pietri, "Optimal Control of Mass Transport Time-Delay Model in an EGR," *SAE Tech. Pap.*, vol. 2020-April, no. April, pp. 1–15, 2020.

[17] D. Bresch-Pietri, T. Leroy, J. Chauvin, and N. Petit, "Practical delay modeling of externally recirculated burned gas fraction for spark-ignited engines," *IFAC Proc. Vol.*, vol. 46, no. 3, pp. 232–237, 2013.

[18] J. Wahlström and L. Eriksson, "Modelling diesel engines with a variable-geometry turbocharger and exhaust gas recirculation by optimization of model parameters for capturing non-linear system dynamics," *Proc. Inst. Mech. Eng. Part D J. Automob. Eng.*, vol. 225, no. 7, pp. 960–986, 2011.

[19] L. Meng, J. Luo, X. Yang, and C. Zeng, "Intake air mass observer design based on extended Kalman filter for air-fuel ratio control on SI engine," *Energies*, vol. 12, no. 18, 2019.

[20] K. Min, J. Shin, D. Jung, M. Han, and M. Sunwoo, *Estimation of Intake Oxygen Concentration Using a Dynamic Correction State with Extended Kalman Filter for Light-Duty Diesel Engines*, vol. 140, no. 1. 2018.

Contact Information

Contact details for the main author should be included here. Details may include mailing address, email address, and/or telephone number (whichever is deemed appropriate).

Acknowledgments

If the Acknowledgments section is not wanted, delete this heading and text.

Definitions/Abbreviations

AFR	Air to Fuel Ratio
AHRR	Apparent Heat Release Rate
BP	Back Pressure
CAC	Charge Air Cooler
CAD	Crank Angle Degree
CI	Compression Ignition
ECU	Engine Control Unit
EGR	Exhaust Gas Recirculation
EKF	Extended Kalman Filter

FPGA	Field-Programmable Gate Array	**PXI**	PCI eXtensions for Instrumentation
HP-EGR	High Pressure EGR	**SI**	Spark Ignition
ICE	Internal Combustion Engine	**UEGO**	Universal Exhaust Gas Oxygen
IMEP	Indicated Mean Effective Pressure	**VGT**	Variable Geometry Turbine
LP-EGR	Low Pressure EGR	**WRAF**	Wide Range Air Fuel sensor

Comments for reviewers

1. Reviewer #: 272598

Very well structured. Grammar, sentence structure and spellings could be improved.

Response:

Thank you very much for your review. The spelling was checked thoroughly as well as the grammar and sentence structure and all the mistakes were corrected.

2. Reviewer #: 276196

Good technical paper that is thoroughly written. Please go through spelling errors and cross-reference errors that are present throughout the paper and fix them: e.g. in page 1, second column, second sentence "In [8] a 6% CO2 reduction was achived...", the word "achived" should be achieved

What are smart NOx sensors? Fast-response sensors with pressure compensation? If so, simply state what they are or put a simple descriptor for what makes those sensors smart.

Please use "test methodology" rather than "test campaign"

Please use "handle" rather than "cope". E.g. third sentence in the LP-EGR line dynamics section: "To cope with this issue..." can be rephrased as "To handle the complex transport phenomena, a black box dynamic model was proposed to estimate the transport mechanisms of species..."

Response:

Thank you very much for your review. The spelling and cross-reference errors were corrected. Your recommendations regarding the vocabulary were taken into consideration.

As for the smart NOx sensor: the word “smart” is the name given by the manufacturers (Continental and NGK) to this generation of NOx sensors because can be directly installed in exhaust gas stream of a combustion engine and can measure NOx components with less interference effect of other gas components, also it is a standalone sensor for ECU, with an integrated in-connector control electronics. Another difference with the previous generation is that Continental replaced the complex, analog control circuits used in the first NOx sensor with a fully digital evaluation unit, the basic principle remains the same, with most differences being in the detail.

(http://www.ngk-detroit.com/23.html)

(https://www.linkedin.com/pulse/nox-sensors-development-echo-diesel-parts-supplier-feng/).